Plasmonics
https://doi.org/10.1007/s11468-024-02302-8

RESEARCH

Fabrication of Gold Thin Films on Cooled Glass Substrates

Melih Manir[1,2,3] · Gamze Genç[1,6] · Vagif Nevruzoglu[3] · Murat Tomakin[4] · Arif E. Cetin[5]

Received: 13 March 2024 / Accepted: 5 April 2024

Abstract
In this article, gold (Au) thin films were fabricated on glass substrates under vacuum conditions (4.5×10^{-6} Torr) within a temperature range of 100–300 K, incrementing in steps of 50 K. Analyses through Field Emission Scanning Electron Microscopy (FESEM) revealed that at a substrate temperature of 230 K, the films featured spherical clusters of uniform size, e.g., 11–12 nm, suggesting that the soliton growth mechanism predominates at this temperature. Atomic Force Microscopy (AFM) further demonstrated that the average surface roughness (Ra) of the Au films varied with the substrate temperature, ranging from 1.2 to 4.7 nm, with the smoothest film observed at 230 K. X-ray diffraction (XRD) analysis confirmed that all films exhibited a cubic crystal structure oriented in the (111) plane. Optical analyses indicated that the films produced across the entire substrate temperature spectrum showed surface plasmon excitation within the 520–600 nm wavelength range. To excite surface plasmons at longer wavelengths, the Au film fabricated at 230 K was annealed at 773 K under vacuum conditions for an hour, enlarging the grain size to ~ 15 nm. Post-annealing, optical measurements revealed a 70-nm shift in the peak position of the plasmonic resonance to a longer wavelength of 650 nm, showcasing the tunable nature of the plasmonic effects through thermal processing.

Keywords Gold nanoparticles · Surface plasmon · Cryogenic effect · Soliton model

Introduction

Gold (Au) nanoparticles play a critical role in the excitation of the surface plasmon resonance (SPR) phenomenon [1–14]. The effectiveness of Au nanoparticles in generating SPR phenomenon within the visible spectrum, e.g., 500–700 nm, has facilitated their use in cutting-edge technologies, spanning from biosensors to solar cells, or even photothermal treatment of cancer cells [4, 5, 14]. However, a review of the literature reveals that the synthesis of Au nanoparticles often involves the use of highly toxic chemical compounds. This presents a significant concern, especially in therapeutic contexts, where such toxicity can lead to adverse side effects [14]. Moreover, an effective realization of the SPR phenomenon metallic nanoparticles must possess a crystal structure comprising clusters of uniform size [8, 15]. Currently, the fabrication of metallic and semiconductor films predominantly employs techniques such as vacuum thermal evaporation, electrodeposition, chemical sputtering, and chemical bath deposition [16, 17]. These methods involve the deposition of materials onto the surface of heated substrates. However, this process often results in the formation of films characterized by islets of varying sizes on the substrate surface [8, 15]. Here, the gaps between these islets within the crystal structure could lead to erratic behaviors in the films produced, posing challenges for achieving consistent and controlled film properties [18–22].

Recently, a groundbreaking approach has emerged for producing metallic and semiconductor films, wherein substrates are cooled to cryogenic temperatures during the deposition process. Films produced using this innovative cryogenic effect method have been shown to exhibit qualities akin to those of single crystals, a notable advancement in material science [8,

✉ Melih Manir
melih.manir@erdogan.edu.tr

1 Department of Energy Systems Engineering, Erciyes University, 38039 Kayseri, Turkey

2 Energy Systems Engineering Program, Graduate School of Natural and Applied Sciences, Erciyes University, 38039 Kayseri, Turkey

3 Department of Energy Systems Engineering, Recep Tayyip Erdogan University, 53100 Rize, Turkey

4 Department of Physics, Recep Tayyip Erdogan University, 53100 Rize, Turkey

5 Izmir Biomedicine and Genome Center, Balcova, 35340 Izmir, Turkey

6 Energy Conversion Research and Application Center, Erciyes University, 38039 Kayseri, Turkey

Published online: 15 April 2024

15, 23–26]. This method facilitates film formation through the soliton growth mechanism, resulting in films composed of uniformly sized nanoclusters. Given these advancements, it becomes increasingly evident that employing the cryogenic effect method to fabricate Au thin films is crucial for achieving effective SPR phenomenon at visible wavelengths. This technique promises enhanced precision and uniformity in the properties of the films, positioning it as a key strategy for advancing applications in plasmonics and beyond.

Gür et al. discovered that in Au films with a grain size of 12–20 nm created via the thermal evaporation method on a quartz substrate, the SPR phenomenon occurred at a wavelength of 520 nm [7]. Their research further indicated that the plasmonic excitations shifted towards the infrared spectrum with increases in grain size and changes in geometric shape due to temperature effects. This aligns with findings from multiple studies in the literature that the occurrence of SPR can vary significantly with the geometry, e.g., spheres or cylinders, size, and material composition of the metallic nanoparticles [27–32]. In a separate study, Kim et al. explored how Au nanoparticles influenced the photovoltaic performance of CdS/CdTe solar cells [4]. By depositing Au nanoparticles on the CdTe surface in varying proportions, e.g., control, 0.13%, 0.25%, 0.5%, 1%, and 2%, using the DC sputtering method, they observed that incorporating 0.5% Au nanoparticles enhanced the plasmonic excitations at a 520-nm wavelength, positively impacting the photovoltaic parameters of the device.

Currently, gold (Au) and silver (Ag) nanoparticles, which are integral to the development of electronic devices leveraging plasmonic effects and in the photothermal therapy of cancer cells, are predominantly synthesized through thermal production methods [33, 34]. Yet, films formed on heated substrates tend to exhibit crystal structures composed of variably sized islands. Studies in the literature highlighted the importance of achieving a crystal structure made up of uniformly sized nanoclusters to facilitate an effective Surface Plasmon Resonance phenomenon. This uniformity is critical for optimizing the plasmonic excitations, which is essential for enhancing the efficiency and effectiveness of plasmonic devices and therapeutic applications [35–39].

In this article, Au nanoparticles were fabricated on glass substrates, with the substrate temperature varied in increments of 50 K across a range from 100 to 300 K. The produced samples were subjected to comprehensive analyses using field emission scanning electron microscopy (FESEM), atomic force microscopy (AFM), X-ray diffraction (XRD), and various optical analysis techniques. FESEM imaging revealed that the soliton growth mechanism was predominant at a substrate temperature of 230 K. Subsequently, the Au layer deposited at this optimal temperature, which demonstrated strong plasmonic excitations at a wavelength of 580 nm, was annealed in a vacuum at 773 K for one hour. This post-deposition treatment resulted in an increase in grain size from 11 to 15 nm, and a noticeable shift in the plasmonic resonances to longer wavelengths, specifically around 70 nm longer, achieving a peak at 650 nm.

Materials and Methods

Cryogenic Temperature Method

In this study, a specialized apparatus, depicted in Fig. 1A, was utilized for the cryogenic effect method, with Fig. 1B–D detailing the steps involved in the production of Au nanoparticles using this setup. The apparatus is designed with two principal sections, e.g., a cooling section and a quartz reactor chamber where saturated vapor conditions are maintained. Upon achieving a vacuum pressure of 4.5×10^{-6} Torr, the glass substrates positioned within the sample holder were cooled via liquid nitrogen, with temperature monitoring conducted through a thermocouple. Once the substrate temperature reached the desired level, the Au was evaporated to create a saturated vapor atmosphere within the reactor part of the setup, as illustrated in Fig. 1B. The interaction between the saturated vapor and the cooled substrate was facilitated through an adjustable window, as shown in Fig. 1C. High-purity metallic Au material (99.999% purity, Sigma-Aldrich®) was employed to deposit thin films (Fig. 1D).

Au nanoparticle layers were then formed on the glass substrates for a duration of 25 s, adjusting the substrate temperature in 50 K increments within a range of 100–300 K. Analysis of the FESEM images from the fabricated films revealed that the anticipated soliton growth mechanism, characteristic of the cryogenic effect method, occurred in the temperature range of 250–200 K. To determine the temperature at which the strongest plasmonic excitation occurred, the film fabrication was refined to 10 K increments, identifying 230 K as the optimal substrate temperature for high SPR activity. To explore the SPR phenomenon at various wavelengths, the Au nanoparticles produced at a substrate temperature of 230 K were subsequently annealed at 773 K for one hour in a vacuum. This treatment led to an increase in grain size, and a shift of the SPR event to longer wavelengths, demonstrating the impact of post-deposition thermal processing on the optical properties of the films.

Calibration of the Cryogenic Temperature Method

In this paper, the results of Au nanoparticles such as structural behavior, surface morphology, roughness, and

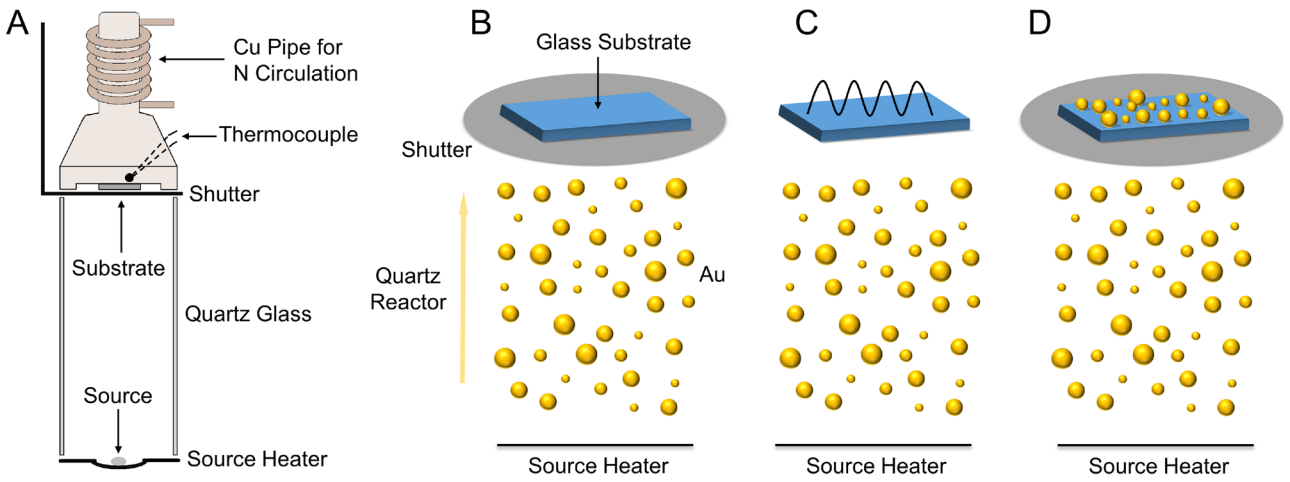

Fig. 1 **A** Schematic illustration of the instrumentation to realize the cryogenic effects, and **B**–**D** the film production stages in the cryogenic temperature method

optical properties were comprehensively examined by a series of advanced analytical techniques. XRD analysis was conducted using a Panalytical Empyrean model instrument equipped with CuKα radiation (λ = 1.5408 Å) to delineate the crystalline structure of the nanoparticles. The surface morphology was scrutinized with a ZEISS GEMINI 500 model FESEM, providing detailed images of the nanoparticles' exterior. To quantify the surface roughness of the samples, a VEECO MULTIMODE 8 AFM was employed, allowing for nanoscale resolution measurements of the surface topography. Optical properties, specifically transmittance (%T), were assessed using a SpectraMax M5 spectrophotometer over the wavelength range of 400–800 nm at ambient temperature, offering insights into the spectral behavior of the Au nanoparticles. Photoluminescence (PL) measurements were performed at an exciting wavelength of 300 nm using SpectraMax M5 spectrophotometer between 325 and 850 nm at room temperature. This holistic approach to characterization ensures a thorough understanding of the nanoparticles' properties, crucial for optimizing their application in various technological and biomedical fields.

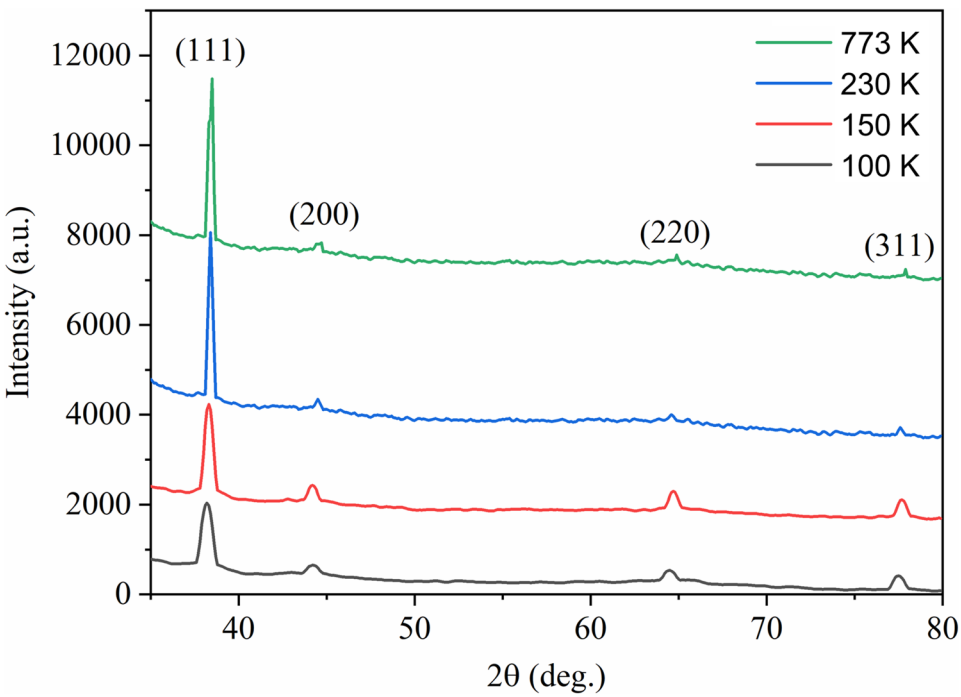

Fig. 2 XRD plots of the samples annealed at 773 K (green), 230 K (blue), 150 K (red), and 100 K (black) substrate temperatures

Results

Figure 2 (green) displays the XRD patterns of Au nanoparticles fabricated at a substrate temperature of 230 K and subsequently annealed at 773 K, together with the XRD plots for Au nanoparticles produced at substrate temperatures of 230 K (blue), 150 K (red), and 100 K (black), respectively, each processed for 25 s. The XRD spectra across these samples reveal reflections from the same crystallographic planes: (111), (200), (220), and (311), indicative of a uniform cubic crystal structure across the different substrate temperatures, as confirmed through comparison with the Joint Committee on Powder Diffraction Standards (JCPDS) database-file 01-075-6560. However, a detailed examination of the XRD spectra uncovers a notable trend, e.g., the intensity of crystallization exhibits a decrease in relation to the substrate temperature. This observation suggests that lower substrate temperatures may impact the crystalline quality or density of the Au nanoparticles, potentially influencing their properties and effectiveness in applications requiring precise crystal structures, e.g., in the enhancement of plasmonic excitations or the fabrication of high-precision electronic devices.

Figure 3 shows the FESEM images of Au nanoparticles synthesized at various substrate temperatures (300 K, 230 K, 100 K) and subsequently annealed at 773 K on glass substrates. FESEM images reveal a significant variation in the surface morphology of the films in relation to the substrate temperature, highlighting the impact of temperature on the growth mechanisms and resulting film structures. For the film produced at a substrate temperature of 300 K, the FESEM image displays a crystal structure comprising grains of varying sizes, ranging from 5 to 30 nm. This heterogeneity in grain size is indicative of the islet growth mechanism predominating at this temperature, where nanoparticles form discrete "islets" before coalescing, leading to a wide distribution in grain sizes. Conversely, the films fabricated at a substrate temperature of 230 K display a more uniform and homogenous surface morphology, with the nanoparticles approximately equal in size, e.g., around 11–12 nm, and spherical in shape. This consistency in particle size and shape suggests that the soliton growth mechanism is

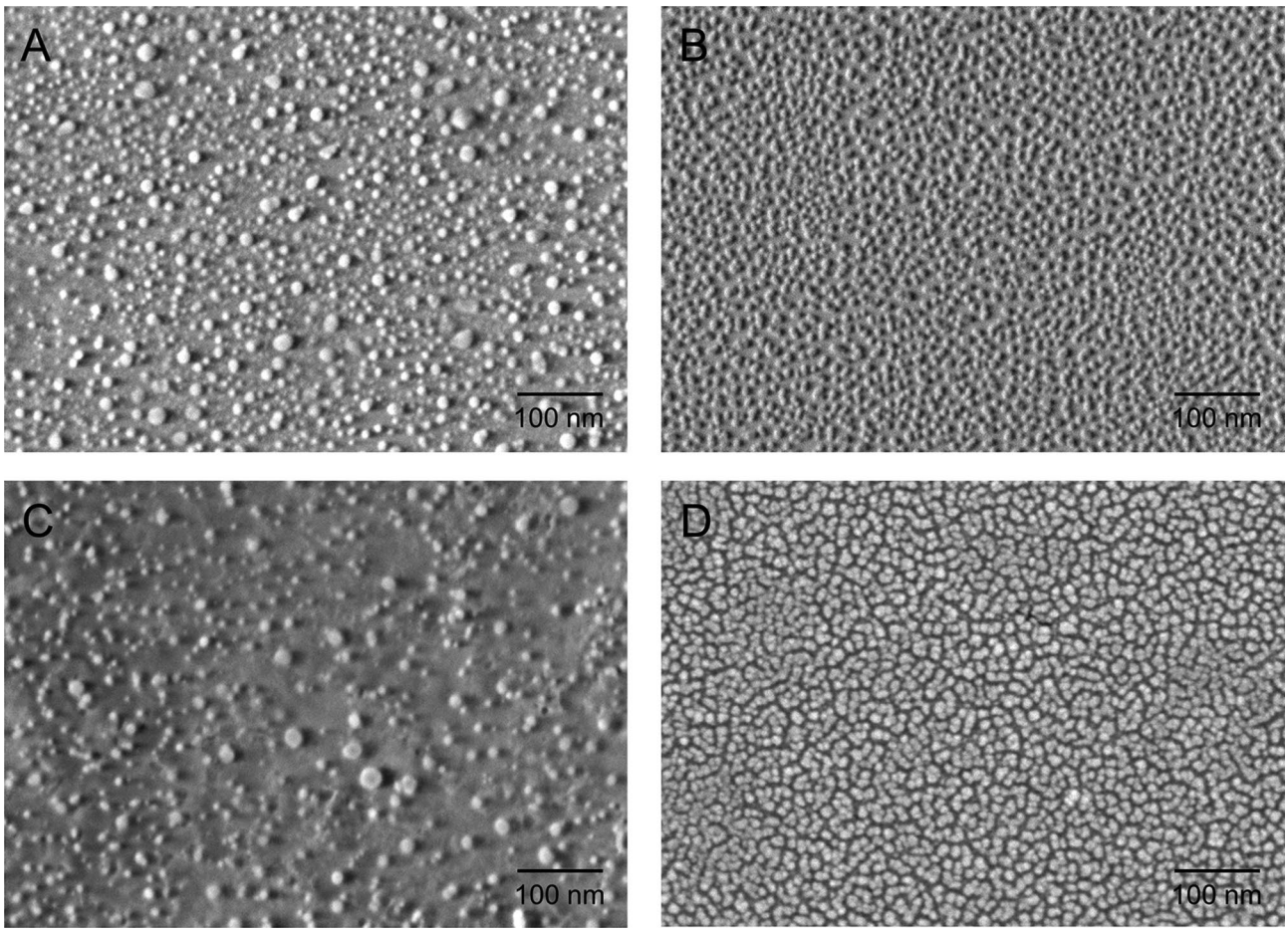

Fig. 3 FESEM images of Au films produced at **A** 300 K, **B** 230 K, **C** 100 K, and **D** the sample annealed at 773 K

Table 1 Parameters calculated from X-ray diffraction patterns of Au films produced on glass at different substrate temperatures for 25 s

Substrate temperature (K)	Degree (°)	d (Å)	a (Å)	B (°)	D (nm)	Strain (ε) $\times 10^{-2}$	Dislocation density (δ) ($\times 10^{14}$ m^{-2})
773 K	38.5	2.336	4.046	0.56	14.681	2.360	46.397
300	38.4	2.341	4.054	0.45	18.345	1.889	29.714
250	38.3	2.347	4.065	0.48	18.340	1.889	29.730
230	38.2	2.353	4.076	0.52	16.297	2.126	37.652
200	38.2	2.353	4.076	0.73	11.283	3.071	78.551
150	38.1	2.359	4.086	0.95	8.625	4.017	134.426
100	37.9	2.371	4.107	1.02	8.141	4.256	150.884

operative at 230 K, enabling a more orderly and compact packing of nanoparticles, which in turn reduces the void distribution on the surface. This tight packing is associated with a higher density of the film, which tends to increase as the substrate temperature decreases further from this optimal point. These observations underline the essential role of substrate temperature in determining the growth mechanism, surface morphology, and structural properties of Au nanoparticle films, with significant implications for their optical properties, electronic applications, and potential use in nanotechnology and materials science.

The analysis of the XRD data yielded key structural parameters for the Au thin films, including the distance between planes (d), lattice parameter (a), particle size (D), strain (ε), and dislocation density (δ), which are summarized in Table 1. FESEM images revealed that as the substrate temperature approached 100 K, both islet and soliton growth mechanisms occurred concurrently during the film formation process. This dual mechanism led to the emergence of grains of varying sizes within the crystal structures of the films, imparting an amorphous characteristic to the structure. A notable observation from the XRD data is the variation in strain values within the crystal structures of the Au thin films, which increased significantly from 1.889×10^{-2} to 4.256×10^{-2} as the substrate temperature was lowered from 300 to 100 K. This variation underscores the fact that by carefully adjusting the deposition temperature, it is possible to tune the strain values within the films. Such tunability is critical for optimizing the physical properties of the films for specific applications, as indicated in the literature [41, 42]. The ability to control strain values is particularly relevant for tailoring the optical and electronic properties of thin films, which can enhance their performance in a wide range of technological applications, including but not limited to, electronics, optics, and materials science.

The grain size distribution of the films produced at varying substrate temperatures, along with the sample annealed at 773 K, are depicted in Fig. 4A–D. Additionally, calculations for particle size and void density derived from FESEM images using the ImageJ software are presented in Table 2. These results reveal a distinct pattern where both grain size, e.g., ranging from 13.399 nm to 7.825 nm, and void density, e.g., 38.963 to 28.589%, decrease as the substrate temperature nears 230 K. This trend suggests an optimal condition for film formation at around 230 K, characterized by relatively uniform and compact grains with minimal void spaces. Interestingly, as the substrate temperature decreases towards 100 K, there is an observed increase in void density to 35.610%. This phenomenon indicates a divergence from the optimal compactness and uniformity achieved near 230 K, likely due to the concurrent presence of islet and soliton growth mechanisms, as previously discussed. This results in a less uniform distribution of grain sizes and an increase in void spaces within the film structure. These findings align with research conducted by Nevruzoglu et al. and Belyaev et al., reporting similar trends in grain size and void density with changes in substrate temperature [8, 40]. Such insights contribute significantly to the understanding of how substrate temperature influences the morphological and structural characteristics of Au thin films, offering valuable guidelines for the controlled synthesis of materials with desired properties for various applications in nanotechnology and materials science.

Figure 5A–D present 3-dimensional AFM images for Au films synthesized at various substrate temperatures, e.g., 300 K, 230 K, and 100 K), and those annealed at 773 K. These images and graphs provide a visual and quantitative analysis of the surface characteristics and roughness variations across the different substrate temperatures. Figure 6 further encapsulates the relationship between the substrate temperature and the average surface roughness (Ra) of the produced films, illustrating this dynamic graphically. This visualization clearly shows that the Ra value exhibits a nearly linear decrease as the substrate temperature is increased from 100 to 230 K, indicating smoother film surfaces at higher substrate temperatures within this range. Surprisingly, beyond 230 K, the Ra value begins to rise again, suggesting an increase in surface roughness. This trend underscores the significant impact of substrate temperature on the morphology of Au films, where a moderate

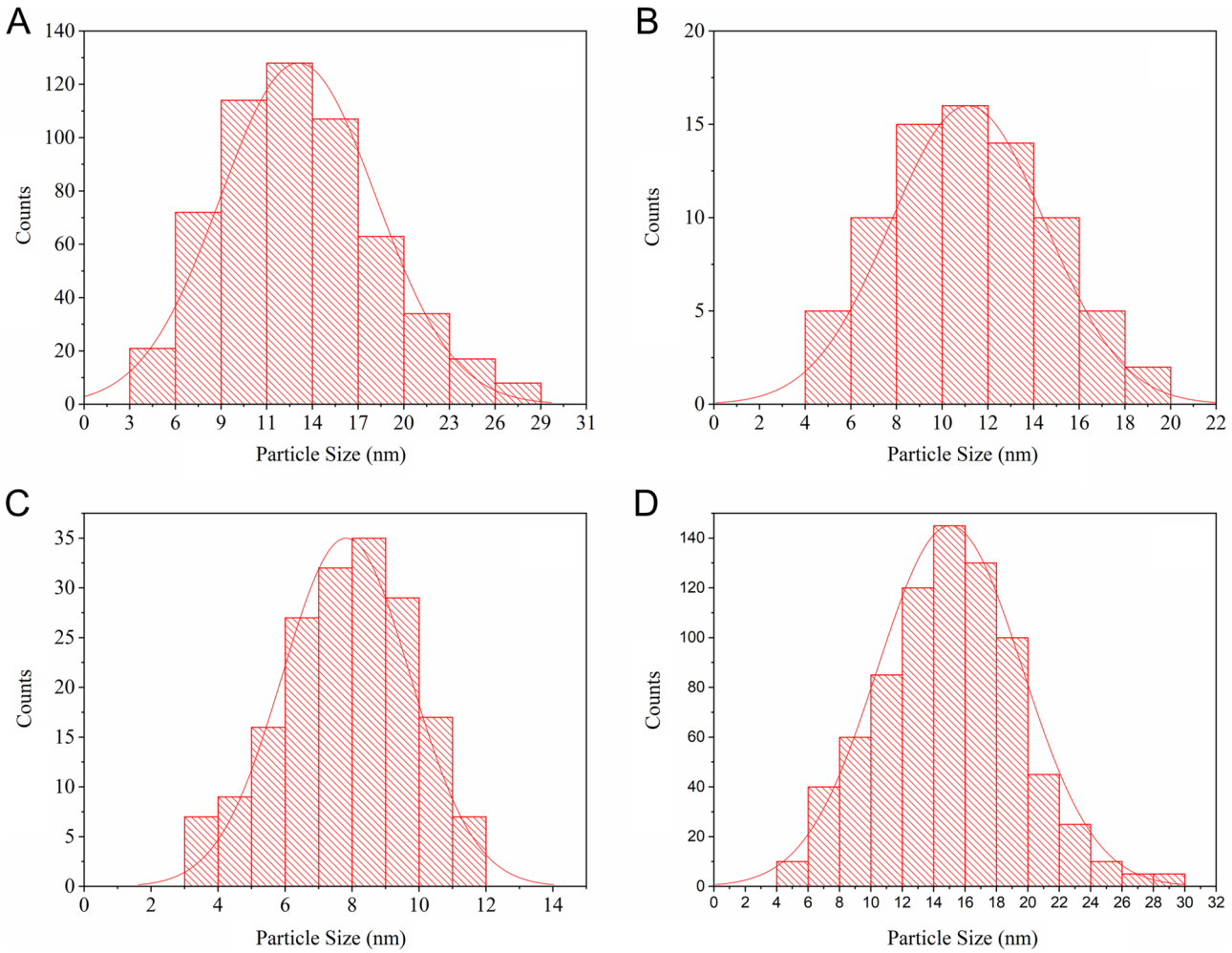

Fig. 4 Grain size distributions of the produced films at **A** 300 K, **B** 230 K, **C** 100 K, and **D** the sample annealed at 773 K

temperature (around 230 K) seems to facilitate the formation of smoother films. Conversely, temperatures either below or above this optimal point lead to increased roughness, likely due to changes in the growth mechanisms and grain structure of the films. The optimal temperature range for achieving minimal surface roughness, as observed, plays a crucial role in applications where surface smoothness is critical, such as in optical devices and sensors, where roughness can affect performance characteristics like reflectivity and sensitivity.

Figure 7A, B demonstrates the optical transmittance and absorbance spectra for Au films fabricated at substrate temperatures of 300 K (black), 230 K (green), and 100 K (red), as well as for the film produced at 230 K and subsequently annealed at 773 K in vacuum (blue). Analysis of these spectra reveals that the strongest plasmonic excitation, e.g., the plasmonic mode supporting the narrowest resonance, occurs at a wavelength of ~ 580 nm when the substrate temperature is at 230 K. This observation aligns with existing research indicating that both the particle size and the specific wavelength at which SPR phenomenon manifest could be finely tuned [7, 9]. Gür et al. discovered that plasmonic excitations in Au films with a grain size

Table 2 Particle size and void density values of the produced films depending on the substrate temperature

Substrate temperature (K)	Particle size (nm)	Void density (%)
773 K	15.037 ± 4.597	29.560
300	13.399 ± 3.408	38.963
250	11.927 ± 3.005	35.896
240	11.520 ± 2.727	32.641
230	11.120 ± 3.390	28.589
220	9.358 ± 2.249	28.756
210	9.077 ± 2.803	28.987
200	8.514 ± 2.685	29.091
150	8.023 ± 2.453	30.093
100	7.825 ± 1.909	35.610

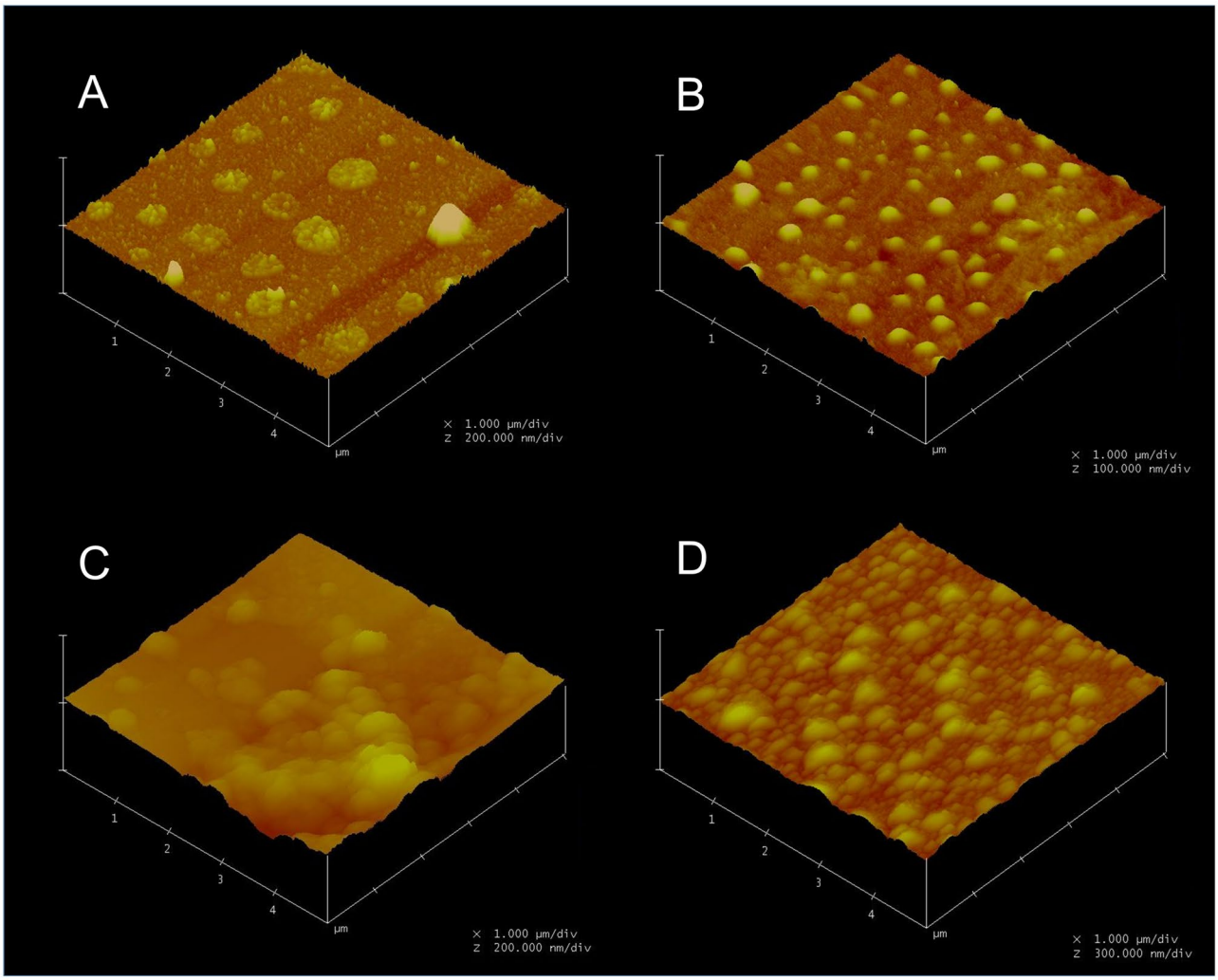

Fig. 5 Three-dimensional AFM images of the samples produced at **A** 300 K, **B** 230 K, **C** 100 K substrate temperature, and **D** the sample annealed at 773 K

of 12–20 nm, created via the thermal evaporation method on quartz substrates, occurred at a wavelength of 520 nm [7]. This finding emphasizes how grain size significantly influences the SPR wavelength. Additionally, they noted that an increase in grain size, triggered by the annealing temperature, along with changes in the geometric shape of the particles, caused the SPR event to shift toward the infrared spectrum. This shift underscores the impact of physical changes within the nanoparticle structure on the plasmonic properties. Kim et al. explored how doping CdS/CdTe solar cells with Au nanoparticles affects the cells' photovoltaic parameters [8]. By introducing Au nanoparticles onto the CdTe surface at varying concentrations (control, 0.13%, 0.25%, 0.5%, 1%, and 2%) through a chemical method, they observed that the SPR phenomenon occurred at 520 nm within the device doped with 0.5% Au nanoparticles. This result further demonstrates the tunability of SPR based on nanoparticle concentration, offering potential enhancements in solar cell efficiency through strategic nanoparticle incorporation. These findings collectively highlight the delicate interplay between nanoparticle size, concentration, and the resulting SPR characteristics, offering valuable insights for optimizing plasmonic and photovoltaic applications through precise material engineering.

Figure 8 presents FESEM images and PL spectra of the Au thin films prepared at substrate temperatures of 230 K, 210 K, and 100 K. Analysis of the PL spectra revealed that all samples exhibited a broad emission around 530 nm. This emission was found to be narrower and more intense for the Au thin film prepared at 230 K (Fig. 8D), attributed to its more uniform and homogeneous surface morphology and grain size distribution (Fig. 8A). The emission range of 500–590 nm for Au, correlating to electronic transitions between the sp band just below the Fermi level and the first

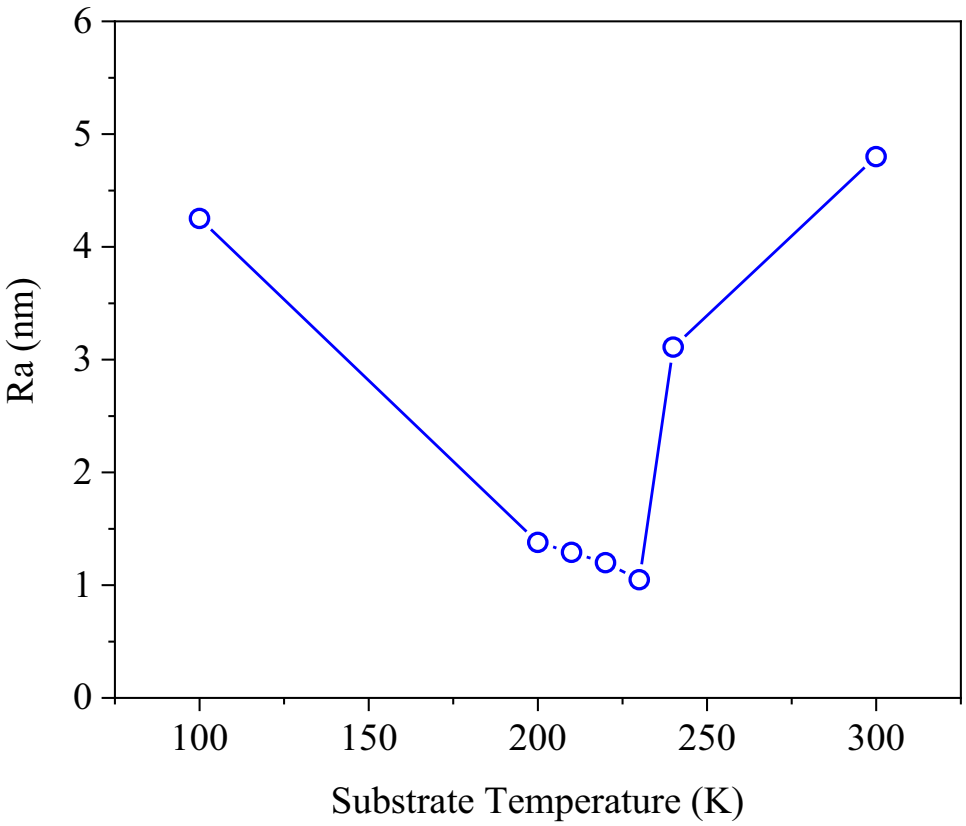

Fig. 6 Average surface roughness values of the produced Au films

d band near point L in the Brillouin zone, has been reported previously [43–47]. The PL spectrum of the Au thin film prepared at 210 K (Fig. 8E) showed distinct emissions around 375 nm, 530 nm, and 750 nm, resulting from the formation of Au nanoparticles of varying sizes (Fig. 8B). Despite the different grain size distribution, the surface morphology and grain shape of the Au thin film prepared at 210 K remained uniform. The emission at 375 nm was both narrower and stronger than the other emissions. This 375 nm emission (3.31 eV) closely matches the theoretical band gap value (3.26 eV) for Au nanoparticles reported by Alluhaybi et al. [48], and a similar band transition observed

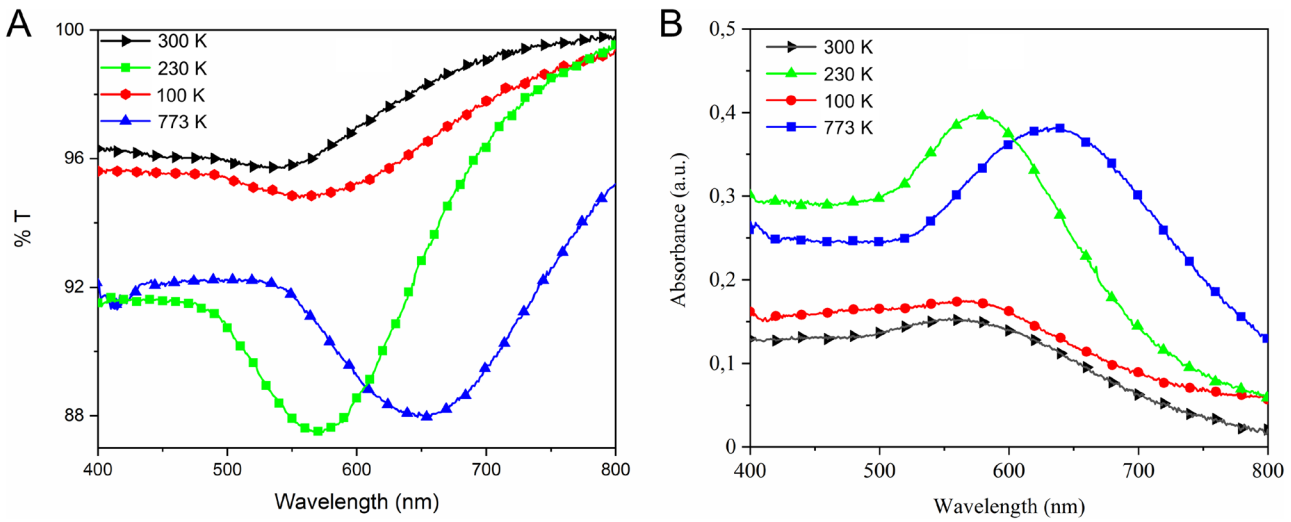

Fig. 7 **A** Optical transmittance and **B** absorbance spectra of Au samples produced at 300 K (black), 230 K (green), 100 K (red), and annealed at 773 K (blue)

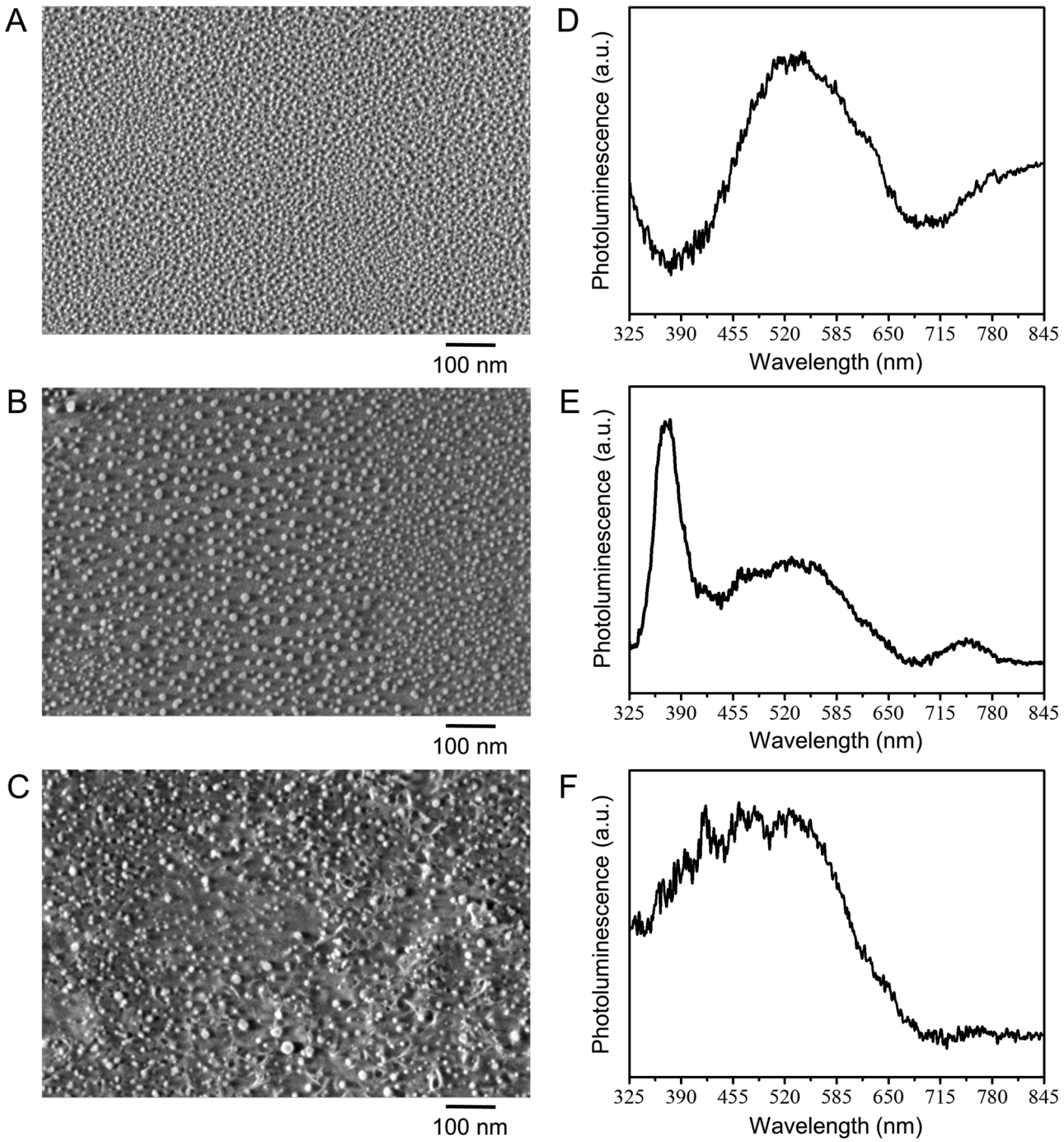

Fig. 8 FESEM images and PL spectra of Au thin films produced at **A**, **D** 230 K, **B**, **E** 210 K, and (**C**, **F**) 100 K

by Desarkar et al. at 354 nm [49]. Gao et al. [50] noted a comparable emission at 750 nm in Au nanobranch structures. For the Au thin film prepared at 100 K, the emission around 530 nm broadened, indicating a loss of homogeneity in grain size, shape, and surface morphology (Fig. 8C). Additionally, as shown in Fig. 8F, low-intensity emissions at around 420 nm, 460 nm, and 480 nm were observed within this broad peak, while emissions at higher wavelengths (> 700 nm) were absent, aligning with findings by Alluhaybi et al. [48]. Consequently, it was concluded that the size, shape, and distribution of Au nanoparticles significantly influence the PL spectra.

Conclusion

In this study, the fabrication of Au nanoparticles on glass substrates was explored over a range of substrate temperatures from 100 to 300 K, increasing in 50 K steps. X-ray diffraction (XRD) analyses demonstrated that all films, regardless of substrate temperature, developed without any foreign phases, exhibiting a pure cubic structure with a preferential orientation in the (111) direction. This uniformity in crystal structure across a broad temperature spectrum underscores the effectiveness of the growth process. Variations were observed in grain size, lattice parameter, and dislocation density, with grain sizes spanning from 18.345 nm to 8.141 nm, lattice parameters ranging from 4.054 to 4.107 Å, and dislocation densities adjusting between 2.9×10^{15} and 15.0×10^{15} m^{-2}. These findings illustrate the substrate temperature's influence on the nanoparticles' microstructural characteristics.

FESEM images highlighted the spherical and uniformly sized clusters of the Au film produced at 230 K, indicating the soliton growth mechanism's activation at this specific temperature. AFM images further supported this, showing a decrease in the average surface roughness (*Ra*) value up to 230 K, after which it increased again. It was shown that the strongest plasmonic excitation was observed at 580 nm, uniquely prominent in the film produced at 230 K. This temperature was pivotal, not only for structural integrity but also for optical properties. Post-annealing of the film at 230 K substrate temperature in a vacuum at 773 K for an hour led to an increase in grain size from 11 to 15 nm, and a notable shift in the SPR event to longer wavelengths by 70 nm, achieving a peak at 650 nm. The PL spectra analysis revealed that all samples exhibited a broad emission centered around 530 nm. Notably, the emission for the Au thin film prepared at a substrate temperature of 230 K was characterized as narrower and more intense. This enhanced emission quality was attributed to the film's homogeneous surface morphology and even distribution of grain size. Our study concludes that it is feasible to produce metallic Au-based nanoparticles on cooled substrates, circumventing the need for toxic chemicals typically employed in nanoparticle synthesis. In conclusion, this methodological advancement opens avenues for safer and environmentally friendly production of nanoparticles, with significant implications for their application in various technological fields.

Author Contributions M.M., G.G., V.N., M.T., and A.E.C. fabricated, and performed the optical and material characterization of the films. All authors prepared and reviewed the manuscript.

Funding This study was carried out within the scope of Erciyes University, Scientific Research Projects Unit Project No. FDK-2022-12367 and with the support of TÜBİTAK 2211/C National PhD Scholarship Program in the Priority Fields in Science and Technology.

Data Availability No datasets were generated or analysed during the current study.

Declarations

Competing Interests The authors declare no competing interests.

References

1. Kusnezh V, Il'chuk H, Kluczyk K, Gwóźdź K, Petrus R, Tsyupko F, Bieganski P, Płaczek-Popko E (2018) Fabrication and photosensitivity of structures based on CdS: Au nanoparticles nanocomposite. J Alloy Compd 746:471–476
2. Shokeen P, Jain A, Kapoor A (2017) Plasmonic ZnO/p-silicon heterojunction solar cell. Opt Mater 67:32–37
3. Rodgersi O (2018) Metal (Ag) nanoparticles on thin film CdS/CdTe solar cells. Locus: Seton Hall J Undergrad Res 1:1–10
4. Kim S, Suh J, Kim T, Hong J, Cho S (2019) Plasmon-enhanced performance of CdS/CdTe solar cells using Au nanoparticles. Opt Express 27:22017–22024
5. Spalatu N, Hiie J, Maticiuc N, Krunks M, Katerski A, Mikli V, Sildos I (2015) Plasmonic effect of spray-deposited Au nanoparticles on theperformance of CSS CdS/CdTe solar cells. Appl Surf Sci 350:69–73
6. Tan H, Santbergen R, Yang G, Smets AHM, Zeman M (2013) Combined optical and electrical design of plasmonic back reflector for high-efficiency thin-film silicon solar cells. IEEE J Photovolt 3:1–6
7. Gür E, Baltakesmez A, Tüzemen S, Yenısoy A (2015) Improved growth quality of the ZnO thin films on Au nano-particles/p-Si. In: IEEE Regional Symposium on Micro and Nanoelectronics (RSM), Kuala-Terengganu, Malaysia, pp 321–324. https://doi.org/10.1109/RSM.2015.7355031
8. Nevruzoglu V, Altuntaş DB, Tomakin M (2020) Cold substrate method to prepare plasmonic Ag nanoparticle: deposition, characterization, application in solar cell. Appl Phys 126:255
9. Koval V, Yakymenko Y, Ivashchuk A, Dusheyko M, Fadieiev M, Didichenko D, Borodinova T (2018) Application of Au Nanoparticles for Silicon Heterojunction Solar Cells. In: 2018 IEEE 38th International Conference on Electronics and Nanotechnology (ELNANO), Kyiv, Ukraine, pp 186–190. https://doi.org/10.1109/ELNANO.2018.8477552
10. Matheu P, Lim SH, Derkacs D, McPheeters C, Yub ET (2008) Metal and dielectric nanoparticle scattering for improved optical absorption in photovoltaic devices. Appl Phys Lett 93:113108
11. Pillai S, Catchpole KR, Trupke T, Green MA (2007) Surface plasmon enhanced silicon solar cells. J Appl Phys 101:1–8
12. Sangnoa R, Maityb S, Mehtac RK (2016) Plasmonic effect due to silver nanoparticles on silicon solar cell. Procedia Comput Sci 92:549–553
13. Wang T, Zou S, Zhu J, Lu Z, Sun H, Ye X, Fang L, Tang R, Su X (2019) Enhancing power conversion efficiency of multicrystalline silicon solar cells by plasmonic effect of Ag nanoparticles embedded in SiNx layer. AIP Adv 9:025218
14. Huang X, Jain PK, El-Sayed IH, El-Sayed MA (2008) Plasmonic photothermal therapy (PPTT) using gold nanoparticles. Lasers Med Sci 23:217–228
15. Manir M, Nevruzoglu V, Tomakin M (2021) The investigation of stability of n-CdS/p-Cu_2S solar cells prepared by cold substrate method. Semicond Sci Tech 36:1–9

16. Würfel P, Würfel U (2016) Physics of solar cells: from basic principles to advanced concepts, 3rd edn. John Wiley & Sons. ISBN: 978-3-527-41312-6
17. George J (1992) Preparation of Thin Films. CRC Press
18. Iacomi F, Purica M, Budianu E, Prepelita P, Macovei D (2007) Structural studies on some doped cds thin films deposited by thermal evaporation. Thin Solid Films 515:6080–6084
19. Lee WJ, Umana-Membreno GA, Dell J, Faraone L (2015) Substrate heating effects on properties of CdS thin films prepared by thermal evaporation for photovoltaic applications. In: 2015 IEEE 42nd Photovoltaic Specialist Conference (PVSC), New Orleans, LA, USA, pp 1–4. https://doi.org/10.1109/PVSC.2015.7355788
20. Somorjai GA, Jepsen DW (1964) Evaporation mechanism of cds single crystals diffusion controlled evaporation of cadmium- and sulfur-doped cds. J Chem Phys 41:1394–1399
21. Mahdi MA, Hassan JJ, Kasim SJ, Ng SS, Hassan Z (2014) Optical properties of cds micro/nanocrystalline structures prepared via a thermal evaporation method. Mater Sci Semicond Process 26:87–92
22. Mahmoud SA, Ibrahim AA, Riad AS (2000) Physical properties of thermal coating cds thin films using a modified evaporation source. Thin Solid Films 372:144–148
23. Nevruzoglu V, Manir M, Ozturk G (2020) Investigation of the electrical properties of Ag/n-Si schottky diode obtained by two different methods. J Ceram Process Res 21:256–262
24. Yuzuak GD, Yuzuak E, Nevruzoglu V, Dincer I (2019) Role of low substrate temperature deposition on Co-Fe thin films. Appl Phys A-Mater Sci Process 125:11
25. Tomakin M, Altunbaş M, Bacaksiz E, Çelik Ş (2012) Current transport mechanism in CdS thin films prepared by vacuum evaporation method at substrate temperatures below room temperature. Thin Solid Films 520:2532–2536
26. Bacaksiz E, Altunbaş M, Yılmaz S, Tomakin M, Parlak M (2007) Effects of CdCl2 treatment on properties of CdTe thin films grown by evaporation at low substrate temperatures. Cryst Res Technol 42:890–894
27. Rehman Q, Khan AD, Khan AD, Noman M, Ali H, Raufd A, Ahmada MS (2019) Super absorption of solar energy using a plasmonic nanoparticle based CdTe solar cell. Royal Soc Chem 9:34207
28. Rahmani A, Vatankhah S (2017) Improving the efficiency of thin film amorphous silicon solar cell by changing the location and material of plasmonic metallic nanostructures. Energy Procedia 141:8–12
29. Enrichia F, Quandt A, Righinia GC (2018) Plasmonic enhanced solar cells: Summary of possible strategies and recent results. Renew Sustain Energy Rev 82:2433–2439
30. Clavero C (2014) Plasmon-induced hot-electron generation at nanoparticle/metal-oxide interfaces for photovoltaic and photocatalytic devices. Nat Photonics 8:95–103
31. Ameen M, Ali KS, Rahman LM, Ali M, Akhtaruzzaman K, Sopiana S, Radiman N, Aminab A (2017) Computational study on the energy bandgap engineering in performance enhancement of CdTe thin film solar cells. Results Phys 7:1066–1072
32. Khan ZR, Zulfequar M, Khan MS (2012) Structural, optical, photoluminescence, dielectric andelectrical studies of vacuum-evaporated CdTe thin films. Bull Mater Sci 35:169–174
33. Ho WJ, Feng SK, Liu JJ, Yang YC, Ho CH (2018) Improving Photovoltaic performance of silicon solar cells using a combination of plasmonic and luminescent downshifting effects. Appl Surf Sci 439:868–875
34. Wen JH, Sheng KF, Jheng JL (2017) Plasmonic effects of silver nanoparticles with various dimensions embedded and non-embedded in silicon dioxide antireflective coating on silicon solar cells. Appl Phys A 124:1–8
35. Fahim N, Ouyang Z, Zhang Y, Jia B, Shi Z, Gu M (2012) Efficiency enhancement of screen-printed multicrystalline silicon solar cells by integrating gold nanoparticles via a dip coating process. Opt Mater Express 2:190–204
36. Ghosh B, Mondal NK, Banerjee P, Pal J, Das S (2002) A method for forming low resistance contact to p–CdTe. IEEE Trans Electron Devices 49:2352–2355
37. Senthilkumar N, Arulraj A, Nandhakumar E, Ganapathy M, Vimalan M, Potheher IV (2018) Green mediated synthesis of plasmonic nanoparticle (Ag) for antireflection coating in bare mono silicon solar cell. J Mater Sci: Mater Electron 29:12744–12753
38. Zhixin L, Ling X, Wengping Z, Zhaoyun G, Jun X, Weining S, Yao Y, Zhongyuan M, Kunji C (2015) Extended short-wavelength spectral response of organic/(silver nanoparticles/Si nanoholes nanocomposite Films) hybrid solar cells due to localized surface plasmon resonance. Appl Surf Sci 334:110–114
39. Choudhury SA, Nawshin N, Chowdhury MH (2017) Influence of particle shape on the efficacy of plasmonic metal nanoparticles to enhance the energy conversion efficiency of thin-film solar cells. In: TENCON 2017 - 2017 IEEE Region 10 Conference, Penang, Malaysia, pp 2393–2398. https://doi.org/10.1109/TENCON.2017.8228262
40. Belyaev AP, Rubets VP, Kalinkin IP (2003) Mater Phys Mech 6:58
41. Ogundare OD, Akinribide OJ, Adetunji AR, Adeoye MO, Olubambi PA (2019) Crystallite size determination of thermally deposited Gold Nanoparticles. Procedia Manuf 30:173–179
42. Singh AK, Srivastava ON (2015) One-step green synthesis of gold nanoparticles using black cardamom and effect of pH on its synthesis. Nanoscale Res Lett 10:353
43. Beversluis MR, Bouhelier A, Novotny L (2003) Continuum generation from single gold nanostructures through near-field mediated intraband transitions. Phys Rev B 68:11
44. Dulkeith E, Niedereichholz T, Klar TA, Feldmann J, von Plessen G, Gittins DI, Mayya KS, Caruso F (2004) Plasmon emission in photoexcited gold nanoparticles. Phys Rev B 70:205424
45. Amran TST, Hashim MR, Al-Obaidi NKA et al (2013) Optical absorption and photoluminescence studies of gold nanoparticles deposited on porous silicon. Nanoscale Res Lett 8:35
46. Yorulmaz M, Khatua S, Zijlstra P, Gaiduk A, Orrit M (2012) Luminescence quantum yield of single gold nanorods. Nano Lett 12:4385–4391
47. Noginov MA, Zhu G, Gavrilenko VI (2007) Sensitized nonlinear emission of gold nanoparticles. Opt Express 15:15648–15655
48. Alluhaybi HA, Ghoshal SK, Alsobhi BO, Wan Shamsuri WN (2019) Visible photoluminescence from gold nanoparticles: A basic insight. Optic 192:162936
49. Desarkar HS, Kumbhakar P, Mitra AK (2012) Linear optical absorption and photoluminescence emission properties of gold nanoparticles prepared by laser ablation technique. Appl Phys A 108:81–89
50. Gao N, Chen Y, Li L, Guan Z, Zhao T, Zhou N, Yuan P, Yao QS, Xu QH (2014) Shape-dependent two-photon photoluminescence of single gold nanoparticles. J Phys Chem C 118:13904–13911